Characterization of Spark Ignition energy transfer by optical and non-optical diagnostics

Carlos Benito Parejo, Quentin Michalski, Camille Strozzi, Julien Sotton, Marc Bellenoue

▶ **To cite this version:**

Carlos Benito Parejo, Quentin Michalski, Camille Strozzi, Julien Sotton, Marc Bellenoue. Characterization of Spark Ignition energy transfer by optical and non-optical diagnostics. 8th european combustion meeting, Apr 2017, dubrovnik, Croatia. hal-01537769

HAL Id: hal-01537769
https://hal.science/hal-01537769

Submitted on 12 Jun 2017

HAL is a multi-disciplinary open access archive for the deposit and dissemination of scientific research documents, whether they are published or not. The documents may come from teaching and research institutions in France or abroad, or from public or private research centers.

L'archive ouverte pluridisciplinaire **HAL**, est destinée au dépôt et à la diffusion de documents scientifiques de niveau recherche, publiés ou non, émanant des établissements d'enseignement et de recherche français ou étrangers, des laboratoires publics ou privés.

Characterization of Spark Ignition energy transfer by optical and non-optical diagnostics

C. J. Benito Parejo[1*], Q. Michalski[1], C. Strozzi[1], J. Sotton[1], M. Bellenoue[1]
[1] Institut Pprime, CNRS, ISAE-ENSMA, Université de Poitiers, F-86962 Futuroscope Chasseneuil, France

Abstract
This study focuses on the measurement of energy deposited in the fluid by an electrical discharge in different test conditions. An experimental setup is developed for this purpose: a transistorized coil system supplies the electrical energy input for the spark, from 25 to 45 mJ, which is measured at a pair of pin-to-pin electrodes. The energy deposit, ranging from 8 to 15 mJ, is measured using two different techniques: constant volume calorimetry, and Speckle-based Background-Oriented Schlieren (SBOS). Efficiency of the energy transfer is estimated. Calorimetry shows that efficiency depends on inter-electrode gap and gas conditions, increasing with pressure and gap. SBOS provides spatial distributions of density field, temperature and enthalpy. Calorimetry and SBOS provide similar results in terms of the rate of energy deposit over time. Different test conditions are obtained changing inter-electrode gap (from 1 to 3 mm), energy input and gas pressure (from 0.5 to 4 bar).

I. Introduction

Spark ignition is a fundamental process for combustion, and has been widely studied [1-10]. New propulsion systems require high power and efficiency for cleaner functioning. Safety issues, such as engine relight in case of a flameout at high altitudes and low pressure, impose severe working conditions. Therefore there is a need for functional ignition systems matching their working conditions. Ignition systems are usually characterized by the electrical energy they use to produce the discharge, although the energy deposit into the fluid is of high importance for combustion and flame formation simulation.

The approach followed in this work consists in the study of this energy deposit and of the energy transfer efficiency at different pressures and conditions. Two different methods are proposed to characterize spark ignition.

Constant volume calorimetry [5] is chosen to study time evolution of energy deposit. It measures the pressure rise inside a closed volume and estimates the heat deposit that caused it. Roth et al. [11] and other authors [2, 3] studied influence of electrode geometry and gas properties in the discharge.

Background Oriented Schlieren (BOS) has been used a lot in a qualitative level, as it has good measurement qualities as wide adaptable sensibility range and acquisition field size. Quantitative measurement is also possible, as for density field [12-15] and temperature in reactive fluids [16]. The use of the speckle of a laser as a background (SBOS) [17] allows fine dynamic tuning over background spatial resolution even at high optical magnification.

II. Specific Objectives

This work aims at characterizing the energy transfer at spark ignition. First, calorimetry and SBOS experimental setups are tested and validated. Then an academic electrical discharge is studied, and energy deposited in the fluid is compared to the electrical energy input to estimate the energy transfer efficiency.

III. Experimental Methods

III.1 Constant volume calorimetry

Energy deposit in the fluid is estimated by the differential pressure rise inside a closed vessel. After high voltage is applied to a pair of electrodes, an electrical discharge takes place. The spark acts as a heat source, and calorimetry is used to measure this energy deposit. In a constant-volume closed vessel, for ideal gas conditions, this thermal energy (E_{th}) can be obtained from the pressure rise. This is represented in Eq. (1), where γ is the capacity ratio and V the chamber volume.

$$E_{th} = \frac{1}{\gamma - 1} \Delta p \, V \quad (1)$$

Electrical energy supplied to the electrodes (E_{el}) is obtained from voltage and current signals as in Eq. (2). Efficiency of the energy transfer (η) is estimated relating the energy deposit E_{th} to E_{el} as defined in Eq. (3).

$$E_{el} = \int I \, U \, dt \quad (2)$$

$$\eta = \frac{E_{th}}{E_{el}} \quad (3)$$

Electrical equipment to perform the tests consists of a pair of pin-to-pin tungsten electrodes (2 mm diameter, conic ends at 22.5°) connected to a commercial Transistorized Coil Ignition system (TCI, "Top Plug" BERU ZSE 041). The Selectronic SL-1730SL20A DC source supplies energy for the system, and a rectangular signal generator is used to trigger the TCI. Electrical measurements are made using a Tektronix P6015A high voltage probe and a

* Corresponding author:
carlos-javier.benito-parejo@ensma.fr

LeCroy CP031 current probe, both plugged close to the electrodes, as in Fig. 1.

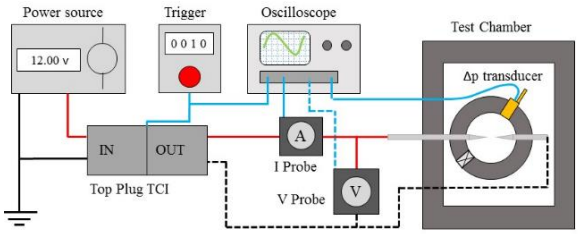

Figure 1: Calorimetry setup

The pressure rise inside the 6 mL test vessel, around 10 mbar, requires high sensitivity equipment, so a differential pressure transducer is chosen. The test vessel is placed inside a 0.5 L chamber to provide the transducer with a reference pressure at stable conditions. Both chambers have transparent sides adapted for visualization measurements. A Meggitt 8510B-1 piezo-resistive differential pressure transducer is used to register the differential pressure rise between the inner and outer volumes. This signal is filtered and amplified by a Meggitt DC Amplifier model 136, which includes a low pass fourth order Butterworth filter with a -3 dB cutoff frequency at 10 kHz. All the signals are registered using a LeCroy waverunner 104Xi high speed sampling oscilloscope, sampling from 200 MHz to 1 GHz at tests.

III.2 SBOS

Speckle-based Background-Oriented Schlieren is based on the variation of the fluid refractive index due to density gradients. An electrical discharge produces a small size hot kernel with strong density variations. Refractive index of those areas varies as in the Gladstone-Dale relation, Eq. (4), where n is the refractive index, ρ is density and G the Gladstone-Dale constant.

$$n - 1 = \rho\, G \qquad (4)$$

The light ray trajectory bending with refractive index gradient is modelled by the eikonal equation, Eq. (5). It can be integrated along the light path, yielding directional components of the schlieren intrinsic angular ray deflection ε, Eq. (6).

$$\begin{cases} \dfrac{\partial^2 x}{\partial z^2} = \dfrac{1}{n}\dfrac{\partial n}{\partial x} \\ \dfrac{\partial^2 y}{\partial z^2} = \dfrac{1}{n}\dfrac{\partial n}{\partial y} \end{cases} \qquad (5)$$

$$\begin{cases} \varepsilon_x = \dfrac{1}{n}\displaystyle\int_{\mathcal{C}} \dfrac{\partial n}{\partial x}\,dz \\ \varepsilon_y = \dfrac{1}{n}\displaystyle\int_{\mathcal{C}} \dfrac{\partial n}{\partial y}\,dz \end{cases} \qquad (6)$$

Observing a reference pattern through the area where the discharge takes place before and after the event, several points would be displaced as in a mirage effect. Comparison of those images is made, applying PIV type data treatment, so the displacement field δ is obtained. Geometrical estimations relate the displacement at the camera sensor δ to the angle of light rays deflection at the phenomenon ε, as in Eq. (7), where M is the optical magnification and l the "defocusing" distance.

$$\vec{\delta} = l\, M\, \vec{\varepsilon} \qquad (7)$$

From equations (4), (6) and (7), displacement field gradient is related to density as in Eq. (8).

$$\frac{n}{GMl}\nabla_{x,y}\vec{\delta} = \Delta_{x,y}\int_{\mathcal{C}} \rho(x,y,z)\,dz \qquad (8)$$

Image processing consists then in obtaining the displacement field δ, differentiate it, and solve the Poisson equation (8) to obtain a planar density field. By retro-projection, the density distribution is obtained in cylindrical polar coordinates. Temperature is directly calculated from density. For a reference temperature T_{ref}, enthalpy H of a control volume $\mathcal{V}$ is obtained by tomography. This is represented in Eq. (9), where c_p is the molar constant pressure heat capacity of the gas, R the perfect gas constant and Λ expression is defined in Eq. (10).

$$H = p\frac{Cp(T_{ref})}{R}\iiint_{\mathcal{V}} \Lambda\big(T(r)\big)dV(r) \qquad (9)$$

$$\Lambda(T) = \frac{C_p(T)}{C_p(T_{ref})} - \frac{T_{ref}}{T} \qquad (10)$$

The optical SBOS setup is represented in Fig. (2). A "speckle" static structured background is produced using a diode-pumped continuous solid-state laser MxL-F (λ = 532 nm, 3W), a collimator and a 1 mm width ground glass. The laser parallel beams are expanded by the collimator and impact the ground glass, where the speckle pattern is formed by scattering effects. Test cell represents the calorimetry chamber. Two lenses and a diaphragm regulate optical parameters as focus distance and magnification. The camera used is a PiMax 1k GenII RB-SG, CCD intensified camera at 1 Hz acquisition frequency.

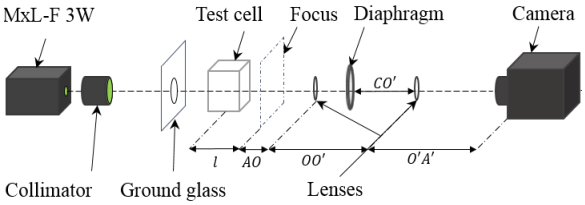

Figure 2: SBOS setup

IV. Results and Discussion

Several aspects of electrical discharges are studied. First, influence of gap distance and pressure over energy and energy transfer is studied by calorimetry. Then spatial distribution of density, temperature and enthalpy are obtained from SBOS and discussed at last. Finally, both experimental techniques are used to analyze energy release over time at the discharge.

IV.1 Energy variation on gap and pressure

Calorimetry tests are performed at different pressures and for different inter-electrode gaps. Chosen initial pressures are 0.5, 1, 2 and 4 bar, for a 1 mm gap. Gap distances of 1, 2 and 3 mm are tested at 0.5 and 1 bar. Global E_{el} and E_{th} at the end of the discharge are presented in Fig. (3).

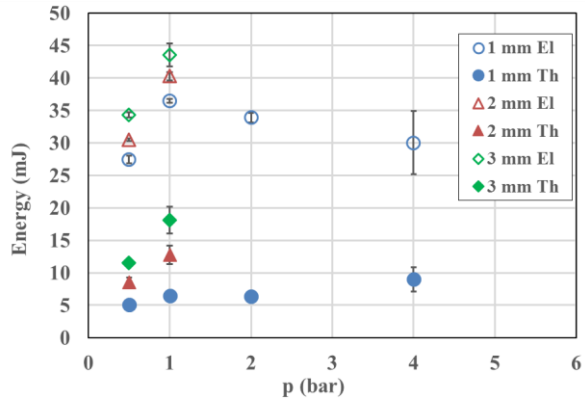

Figure 3: Electrical and thermal energy deposit at different gap and pressure values.

Energy deposit increases for higher gap distance: at 0.5 bar, from 5 mJ at 1 mm gap to 12 mJ at 3 mm gap; and for a pressure of 1 bar, from 7 to 18 mJ at 1 to 3 mm gap. This is explained by the fact that more energy is required to ionize the fluid (higher breakdown voltage) as the conductive channel is longer (REF). Pressure increase also allows a higher energy deposit, e.g. for 1 mm gap at 0.5 to 4 bar.

Efficiency follows same trends, as it can be observed in Fig. (4). It ranges from 27 % at 2 mm gap to 34 % at 3 mm for 0.5 bar of pressure, and from 32 % efficiency to 40 % at 1 bar. For the 1 mm gap, efficiency ranges from 17 % at 1 bar to 30 % at 4 bar, thought there is low influence of pressure under 2 bar.

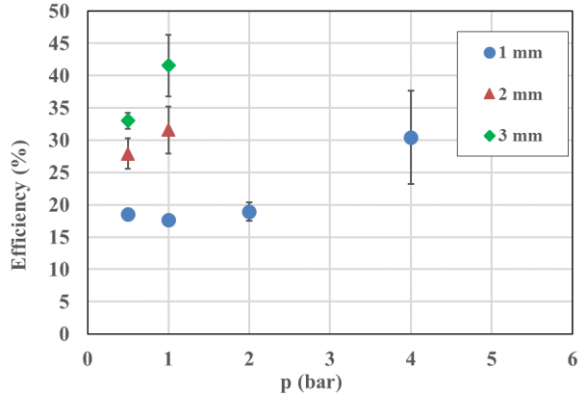

Figure 4: Efficiency at different gap and pressure.

IV.2 Spatial distribution of physical properties

Physical properties of the gas are studied by SBOS at the end of the discharge, i.e. with a 2.5 ms delay. Location of the hot kernel between electrodes is represented as the displacement field divergence of the speckle pattern in Fig. (5). Electrodes are represented masked as used for data processing, to represent their position. Inter-electrode gap is 2 mm, supplied E_{el} is 34.6 mJ and pressure equals 1 bar.

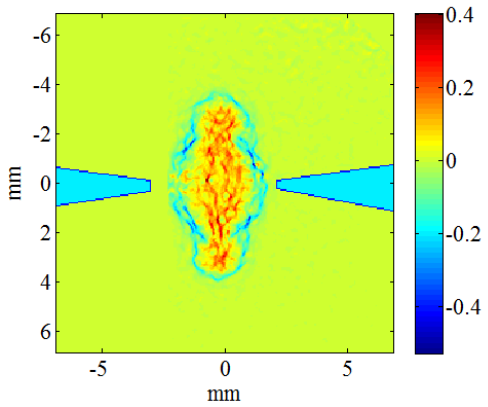

Figure 5: Displacement field divergence at t =2.5 ms (pixel/pixel).

The hot kernel presents a spherical center and a toroidal lobe, due to gas dynamics. Integrating the displacement field and Poisson equation (8), density planar field is obtained. As the discharge is supposed axisymmetric, 3D distribution is estimated by retro-projection of the planar density field. A tomographic view of the resulting relative density field is reported in Fig. (6). This figure represents density difference value from reference ambient density, 1.225 kg/m^3.

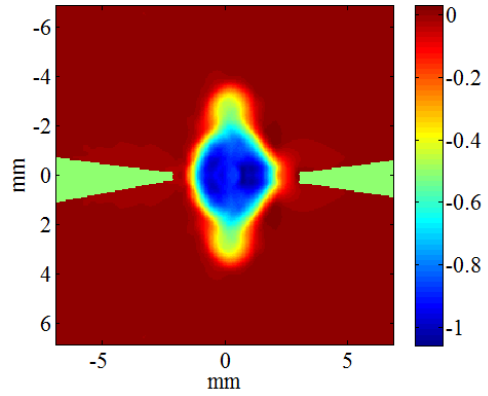

Figure 6: Relative density field (kg/m^3) at t =2.5 ms.

Temperature field is obtained using ideal gas equation. For a reference temperature of 290 K, temperature distribution in the hot kernel reaches 1900 K close to electrode tip, see Fig. (7).

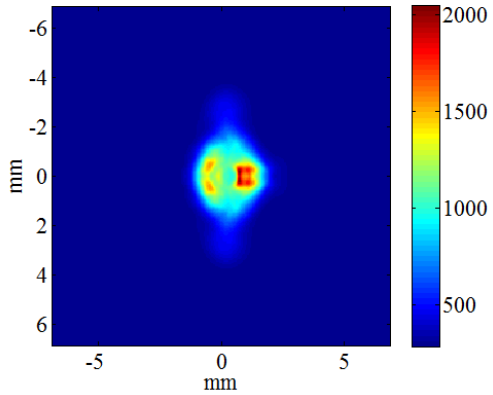

Figure 7: Temperature field (K) at t =2.5 ms.

Finally, temperature field is integrated to obtain the local energy field. Energy distribution is shown in Fig. (8). For this test conditions and a temperature dependant c_p model, total energy resulted in 12 mJ for the 2 mm gap.

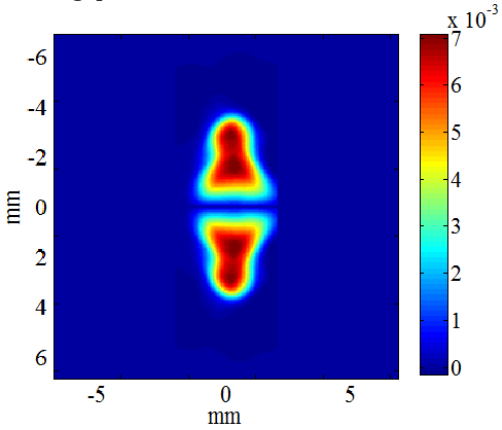

Figure 8: Local energy field (J/m^3) at t =2.5 ms.

IV.3 Energy release over time

Time evolution of energy release over the discharge duration is shown in Fig. (9). Tests are performed at 1 bar and 2 mm gap and saturated TCI coil, resulting in a 2.5 ms discharge duration. Using calorimetry, energy deposit can be measured over time for each test. SBOS only allows measurement of energy at the time of the recorded image for each discharge, so different delay times corresponding to different tests are necessary to investigate global time evolutions.

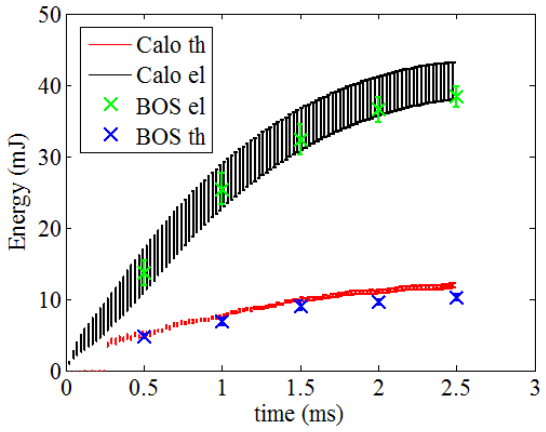

Figure 9: Energy over time, obtained by calorimetry and SBOS

Thermal energy deposit E_{th} ranges from 5 mJ 0.5 ms after the discharge starts to 11 mJ at the end of the discharge, as it can be observed in figure 9. Error bars represent results scattering for the 10 tests performed (10 for calorimetry, 10 for each time measured by SBOS). Efficiency decreases over time, see Fig. (10), and is stabilized at a value of 32 %. This is due to more efficient energy transfer processes at the first phases of the discharge [1, 2]. Results for calorimetry and SBOS are in good agreement.

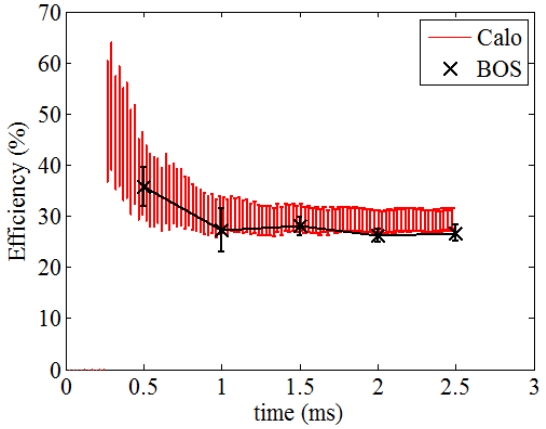

Figure 10: Efficiency over time by calorimetry and SBOS

Conclusions

Electrical discharges were studied by both constant volume calorimetry and Speckle-based Background Oriented Schlieren. Calorimetry tests showed that energy deposit and efficiency increase for tests at longer inter-electrode gap distance or higher pressure. Gas density, temperature and local energy distributions were obtained by SBOS at the end of the discharge. Measurements by SBOS and calorimetry for a reference discharge showed good agreement for energy and efficiency results. Both methods can be used to characterize new ignitors and their performances under different conditions.

Acknowledgements

Authors thank André Agneray for his useful advice for this work. Nouvelle Aquitaine Region,

CAPA ANR Chair, and DGA Radiμs project, are acknowledged for their financial support.

References

[1] R.R. Maly, Fuel Economy in Road Vehicles Powered by Spark Ignition Engines, Plenum Press, 1984.
[2] R.R. Maly, R. Herweg, in Flow and Combustion in Reciprocating Engines, C. Arcoumanis, T. Kamimoto, ed. Springer (2009) 1-66.
[3] K. Eisazadeh-Far, F. Parsinejad, H. Metghalchi, J.C. Keck, Combust. Flame 157 (2010) 2211–2221.
[4] D. Verhoeven, Experiments in Fluids 28 (2000) 86-92.
[5] R.E. Teets, J.A. Sell, SAE paper 880204 (1988).
[6] A. Starikovskiy, N. Aleksandrov, Progress in Energy and Combustion Science 39 (2013) 61-110.
[7] S. Kumagai, T. Sakai, N. Yasugahira, Combustion Science and Technology 6 (1972) 233-239.
[8] P.R. Smy, R.M. Clements, J.D. Dale, D. Simeoni, D.R. Topham, Journal of Physics (1983) 783-791.
[9] B. Sforzo, A. Lambert, J. Kim, J. Jagoda, S. Menon and J. Seitzman, Combustion and Flame (2015) 181-190, 2015.
[10] M. Bellenoue, S. Labuda, B. Ruttun, J. Sotton, Combustion Science and Technology 179:3 (2007) 477-496.
[11] W. Roth, P.G. Guest, G. von Elbe, B. Lewis, J. Chem. Phys. 19 (1951) 1530–1535.
[12] G. E. Elsinga, B. W. van Oudheusden, F. Scarano, D. W. Watt, Exp Fluids 36:2 (2004) 309-325.
[13] M.J. Hargather, G.S. Settles, Opt Laser Eng 50:1 (2012) 8-17.
[14] G.E.A. Meier, L. Venkatakrishnan, Exp Fluids 37:2 (2004) 237-247.
[15] M. Ota, K. Hamada, K. Maeno. Quantitative 3D density measurement of supersonic flow by colored grid background oriented schlieren technique, 27th International Congress of the Aeronautical Sciences (2010)
[16] E.D. Iffa, A.R.A. Aziz, A.S. Malik, Journal of Applied Sciences 11:9 (2011) 1658-1662.
[17] A. H. Meier, T. Roesgen, Exp Fluids 54:6 (2013) 1549